Optimizing resetting of superconducting qubits

Ciro Micheletti Diniz,[1] Rogério Jorge de Assis,[1] Norton G. de Almeida,[2] and Celso J. Villas-Boas[1]
[1]*Departamento de Física, Universidade Federal de São Carlos, 13565-905, São Carlos, São Paulo, Brazil*
[2]*Instituto de Física, Universidade Federal de Goiás, 74.001-970, Goiânia, Goiás, Brazil*

(Received 20 April 2023; accepted 19 October 2023; published 13 November 2023)

Many quantum algorithms demand a large number of repetitions to obtain reliable statistical results. Thus, at each repetition it is necessary to reset the qubits efficiently and precisely in the shortest possible time, so that quantum computers actually have advantages over classical ones. In this work, we perform a detailed analysis of three different models for information resetting in superconducting qubits. Our experimental setup consists of a main qubit coupled to different auxiliary dissipative systems, which are employed in order to perform the erasure of the information of the main qubit. Our analysis shows that it is not enough to increase the coupling and the dissipation rate associated with the auxiliary systems to decrease the resetting time of the main qubit, a fact that motivates us to find the optimal set of parameters for each studied approach, allowing a significant decrease in the reset time of the three models analyzed.

DOI: 10.1103/PhysRevA.108.052605

I. INTRODUCTION

Beyond high-fidelity preparation of the qubit initial states [1,2] and the possibility of implementing error-correction algorithms [3–6], a key step in building an operational quantum computer is the capacity to make these devices process data as quickly as possible. Due to the probabilistic character of the quantum mechanics, many quantum algorithms demand a large number of repetitions, and consequently, the resetting of the qubits must be repeated many times. In this sense, a strategy to speed up the computing is the optimization of the reset process through the elaboration of a fast way to make the qubits return to their initial states. To illustrate the significance of reinitializing the system to the entire process of running an algorithm, in Ref. [7] a set of N coupled linear differential equations was solved, and the solution was mapped to the final state of n qubits (with $N = 2^n$), such that, to achieve a precise solution, it is necessary to repeat the measurements up to $O(2^n)$ times since there are 2^n possible states for the qubits. For instance, we estimate that to solve a set with 1 trillion coupled differential equations it would be necessary to repeat the measurements around 1 trillion times. In this process, if we consider a realistic reset time as in Refs. [8,9], which is of the order of hundreds of nanoseconds or even a few microseconds, it would take some tens of or even a few hundred hours in the reinitialization steps of the system. In order to create a faster resetting, several approaches can be applied. One of them consists of performing measurements on the qubits to invert their states using controlled-duration pulses [10–13]. Other ways to produce an efficient reset process use thermal baths to stabilize the system in a specific final state [14,15] and engineer light-matter interactions either by pulses with a specific frequency interval [16] or by employing an additional level and coupling the qubit to an auxiliary dissipative cavity mode [8].

Looking at the fastest way to reset systems, we analyze here two configurations that use dissipative effects to reset the qubit. In addition, we optimize the reset model from Ref. [8] and compare its results with the ones achieved with the other two models. The different experimental setups, which will be explored throughout this paper, are indicated in Figs. 1(a)–1(e). The first configuration studied here [Fig. 1(c)] is a work qubit (named the main qubit) coupled directly to a second highly dissipative qubit (auxiliary qubit). In Refs. [17,18], a similar model was used to study how to speed up the resetting and purification of the system, but different from the present work, the authors employed a tunable frequency qubit as the main system and considered the presence of correlations between the qubit and the environment. Also, Ref. [19], using a model similar to last one, studied how increasing the size of the ancilla qubit Hilbert space affects the resetting time. In the second configuration [Fig. 1(d)], the main qubit is coupled to a second one which is then coupled to a dissipative cavity mode. Reference [20] also used two auxiliary components as in our model but, once again, considered tunable frequencies in order to maximize the efficiency of the resetting. Finally, in the third experimental setup investigated here we take into account the multilevel structure of a superconducting device; that is, in addition to the two levels that work as the main qubit, an auxiliary third level is considered that is used to couple the quantum device to a dissipative bosonic field mode [Fig. 1(e)]. This resetting mechanism is quite interesting because of its simplicity and efficiency, and it was studied before in Refs. [8,21], where the authors employed a Jaynes-Cummings-type interaction to reset the system but used different approaches, which made the resetting time achieved in the latter more than twice as fast as in the former. Concerning the last configuration, besides saving space in a quantum computer by eliminating the need for an auxiliary qubit, this scheme can be applied to fixed-frequency qubit architectures, as in the case of the IBM systems in Refs. [8,22].

In this work we carry out a numerical analysis of the main qubit dynamics for the three configurations cited above, and then we perform an optimization for each setup, searching

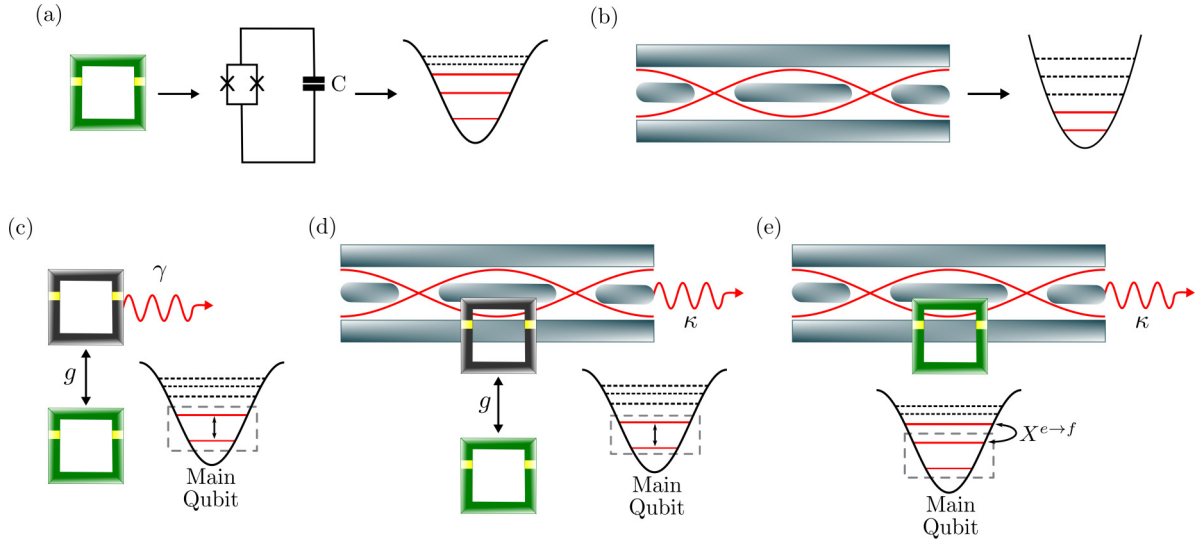

FIG. 1. Pictorial representation of the proposed schemes for resetting the work qubit. (a) shows a superconducting device; our main qubit; its equivalent circuit, composed of a capacitor (C) and two Josephson junctions, which work as a nonlinear inductor; and the respective anharmonic potential with the corresponding energy levels associated with the circuit. (b) shows the waveguide (cavity mode) with the corresponding harmonic potential and energy levels. (c) shows the coupling between the main (green) and dissipative (black) auxiliary qubits, with coupling strength g. The dissipative qubit has damping rate γ. (d) shows the main qubit coupled to the auxiliary one, with coupling strength g. The auxiliary qubit is then coupled (coupling strength λ) to a dissipative cavity mode, whose dissipation rate is κ. (e) shows the qubit with an auxiliary level, which is coupled to the dissipative bosonic mode with damping rate κ.

for the set of parameters that makes the resetting process faster. To present our results, this paper is organized as follows: Sec. II introduces the three models shown in Fig. 1 and describes two different approaches that will be used in the information erasure: (i) the pulsed and (ii) steady-state approaches. Section III shows the parameters that optimize the resetting for each model using these two approaches and discusses their experimental feasibility. Finally, Sec. IV presents our conclusions.

II. DESCRIPTION OF THE MODELS

To model the resetting mechanism we resort to the open quantum system treatment, working in a regime where the interaction energy between the subsystems that make up our setup is much smaller than the free energy of the subsystems themselves. On the other hand, the coupling strengths between the subsystems can be either stronger or weaker than their dissipation rates, usually called strong- and weak-coupling regimes, respectively. In these regimes, assuming the Born and Markov approximations, the dynamics of the system is governed by the master equation ($\hbar = 1$) [23]

$$\frac{\partial \rho}{\partial t} = -i[H, \rho] + L_F(\rho) + L_A(\rho), \tag{1}$$

in which the Hamiltonian H describes the system coupled to the auxiliary components, ρ is the density operator of the composed setup, $L_F(\rho) = \frac{\kappa}{2}(2a\rho a^\dagger - a^\dagger a\rho - \rho a^\dagger a)$ describes the dissipation in a quantum bosonic mode, and $L_A(\rho) = \frac{\gamma}{2}(2\sigma_-^A\rho\sigma_+^A - \sigma_+^A\sigma_-^A\rho - \rho\sigma_+^A\sigma_-^A)$ describes the energy loss of an ancilla qubit. The decay rate of the auxiliary qubit and the bosonic mode are given by γ and κ, respectively, σ_+^A (σ_-^A) is the Pauli raising (lowering) operator for the auxiliary qubit, and a ($a^\dagger$) is the annihilation (creation) operator for the dissipative field mode. Since Eq. (1) is a general equation, it can be used to describe the three configurations studied here; therefore, the Hamiltonian H and the presence of the dissipation operators in this equation will depend on the model, which will be detailed when we formally introduce each setup. Once we know the configuration that will be analyzed, we are able to insert in Eq. (1) the corresponding Hamiltonian that will rule the dynamics in each case and the respective dissipation operators of the auxiliary components and then proceed with the simulations. At this point, one might notice the lack of dissipation operators for the main qubit, our system. In this paper, its absence is a reasonable assumption because quantum computing requires qubits with negligible decay rates; thus, we are considering the main qubit as a nondissipative system, and hence, the entire process of energy dissipation takes place via auxiliary components.

The three configurations for resetting the main qubit that we are going to study here are pictorially represented in Fig. 1. In Fig. 1(a) we represent a superconducting device whose two lower levels represent our main qubit. In Fig. 1(b) we represent the waveguide, which works as a dissipative cavity mode, and it is described by a harmonic potential. In Fig. 1(c) we represent the two-qubit model, in which the main qubit is coupled to an auxiliary dissipative one. In Fig. 1(d), we represent the main qubit coupled to a second one, which in turn is coupled to a dissipative bosonic mode. Finally, in Fig. 1(e), we display the system studied in Ref. [8], which is composed of the main qubit and the auxiliary third level that is coupled to a dissipative cavity mode.

To start, let us introduce the first configuration, as shown in Fig. 1(c), here called the two-qubit model. This setup contains the main qubit coupled to a dissipative auxiliary one and

has the advantage of being very simple and compact, saving space in a quantum computer. Also, the auxiliary qubit does not need to be fully controllable since we do not perform operations over its states. On the other hand, as it can emit in any direction, its dissipation could affect the work qubits in a huge quantum computer, depending on the configuration. In addition, to avoid extra noise and undesired dissipation in the main qubit during the execution of a given quantum process, we must be able to turn its interaction with the auxiliary qubit on and off. This can be done by assuming that the main qubit is frequency tunable and most of the time is very far from resonance with the auxiliary qubit. Then, to implement the reset process we turn its frequency on resonance with the auxiliary qubit, which can be done very quickly, in less than 1 ns [24], so we disregard this time in our analyses. Thus, during the reset process we can consider these qubits to be resonant ones; their Hamiltonian in the interaction picture is given by

$$H_{Q_M-Q_A} = g\big(\sigma_{eg}^{M}\sigma_{ge}^{A} + \text{H.c.}\big), \tag{2}$$

where g is the coupling strength between the main (M) and auxiliary (A) qubits and $\sigma_{ij}^{K} \equiv |i\rangle\langle j|$ is the transition-level operator from level j to level i ($i, j = g, e$) for qubit K ($K = M, A$).

The second configuration analyzed here, named the two-qubit–cavity model, is shown in Fig. 1(d), and it is composed of the tunable (as in the previous case) main qubit coupled to a second nondissipative auxiliary qubit, which in turn is coupled to a dissipative cavity mode field whose dissipation rate is κ. In this model, when turning the main qubit on resonance with the auxiliary one and the cavity mode, we end up with the coupling strength g between the two qubits, which can be different from the coupling strength λ between the auxiliary qubit and the cavity mode field. In this case, in the interaction picture, the Hamiltonian reads

$$H_{Q_M-Q_A-F} = g\sigma_{eg}^{M}\sigma_{ge}^{A} + \lambda\sigma_{eg}^{A}a + \text{H.c.}, \tag{3}$$

where a ($a^\dagger$) is the annihilation (creation) operator for the mode and, again, M and A stand for the main and auxiliary qubits, respectively. This model requires more elements and space, but the dissipative mode can direct the dissipated energy, thereby avoiding disturbances to neighboring working qubits in a quantum computer.

Figure 1(e) shows the third model studied here, in which the main qubit has an auxiliary level that is coupled to a dissipative bosonic mode. This configuration is here called the IBM model since it was studied by IBM researchers [8,25,26]. The Hamiltonian that describes this setup in the rotating frame of the driving field, which has a frequency ω_d, is

$$H_{\text{IBM}} = \delta_c a^\dagger a + \delta_q b^\dagger b + \frac{\alpha}{2} b^\dagger b^\dagger bb + \left[\tilde{g} ab^\dagger + \frac{1}{2}\Omega(t) b^\dagger + \text{H.c.}\right], \tag{4}$$

where a ($a^\dagger$) is the cavity-mode-field annihilation (creation) operator as in the previous case; b ($b^\dagger$) is the annihilation (creation) operator of the main system, now considered a multilevel structure; $\tilde{g}$ is the coupling strength between the cavity and the system; $\Omega(t)$ is the time-dependent amplitude of the microwave field that drives the qubit; $\delta_c = \omega_c - \omega_d$ and $\delta_q = \omega_{ge} - \omega_d$, with ω_c (ω_{ge}) being the transition frequency of the cavity mode (qubit); and, finally, α is the anharmonicity that modifies the frequency transition ω_{ef} between the excited state $|e\rangle$ of the qubit and the auxiliary level $|f\rangle$, such that $\omega_{ef} = \omega_{ge} - \alpha$.

In contrast to the first two configurations, in which the reset processes start when the main qubit begins its interaction with the other components, the resetting in the IBM model occurs in two steps: (i) the state population initially in $|e\rangle$ is transferred by an electromagnetic pulse to the ancilla level $|f\rangle$; (ii) then the population of state $|f\rangle$ is transferred to a dissipative cavity mode via its coupling to the transition $|g\rangle \leftrightarrow |f\rangle$ with the help of a driving field with amplitude $\Omega(t)$ and frequency ω_d. In the first step, the time to transfer the population depends on the intensity of the pulse, i.e., its Rabi frequency, such that the higher the Rabi frequency is, the smaller the time to reach the desired final state is. However, we cannot increase the intensity indiscriminately since levels higher than $|f\rangle$ could be populated in a way that would make step (ii) and, consequently, the entire reset process ineffective. To avoid this loss of efficiency, we will consider here the same pulse that was used in Ref. [8] to transfer the population to the auxiliary level, which causes the first step of the approach to finish in 75 ns. Hence, in order to speed up the resetting for this configuration, we will focus on optimizing the second step by searching for parameters that dissipate the energy faster.

Besides the three configurations, we also deal with two approaches. In the first, here called the steady-state approach, the reset occurs when the system reaches the ground state in a stable way. In the second approach, which we will call the pulsed approach following Ref. [8], the reset occurs when the interaction dynamics takes the main qubit to the ground state for the first time and, exactly at that moment, the pulse is turned off and the information is erased. The IBM model was developed based on only a pulsed approach. As explained before, the model studied in Ref. [8] involved two steps. On the other hand, for the other two models studied here, the pulsed approach happens just in one step since we do not have to transfer the population to another level like in the IBM model. Hence, for the other two models, in the pulsed approach the reset process starts when the main qubit is coupled to the auxiliary dissipative systems, and it is finished when the required ground-state population is achieved for the first time. The time to couple (decouple) the main qubit to (from) the auxiliary components is negligible in the analyses of the reset time, as discussed above.

Now, given the models in Fig. 1, we can proceed with the calculations. For comparison purposes, in all simulations we considered the main qubit to be initially in the excited state, while all the other auxiliary components were considered to be in their respective ground states. In fact, considering the auxiliary components to be in their ground states is a realistic assumption according to [27] since, following their parameters for the mode transition frequency and temperature, the fidelity between the thermal state and ideal ground state is above 99%, which is a small error in the state preparation. Next, we solve Eq. (1) numerically in PYTHON using the QUTIP toolbox [28,29] considering the particularities of each model and analyze the dynamics of the ground-state population of

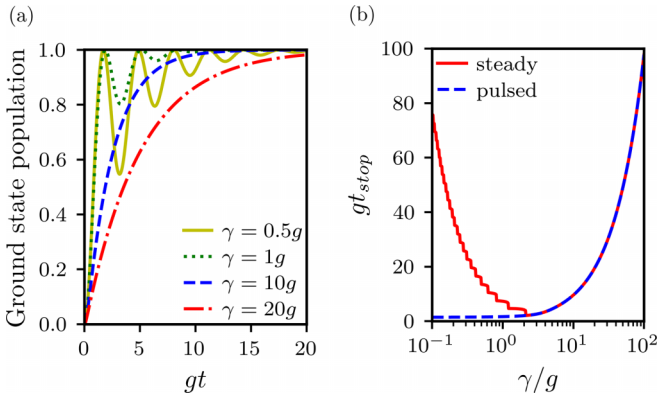

FIG. 2. Resetting process for the two-qubit model. The initial state of the main qubit is $\rho_M = |e\rangle\langle e|$, while the initial state of the auxiliary qubit is $\rho_A = |g\rangle\langle g|$. (a) shows the ground-state population of the main qubit as a function of the dimensionless time gt for different values of the dissipation rate γ (see the legend). (b) shows the dimensionless time gt_{stop} needed to complete the reset as a function of the dissipation rate γ/g for two reset approaches: the pulsed approach (dashed blue line) and the steady-state approach (solid red line).

the main qubit. Studying this property of the main system allows us to determine how and when the reset process must happen.

III. RESULTS AND DISCUSSION

As we are looking at the resetting process, the baseline studied here will be the ground-state population of the main qubit. In this way, for the steady-state approach, we consider the reset process performed when the population of the main qubit reaches the minimum value $p_g = 0.98$ without recurring anymore. Usually, to reset properly, quantum computers require a much higher population in the ground state. However, we decided to choose this value in order to perform a fair comparison of our results with the ones presented in [8], which use this population value for the ground state. In the same way, for the pulsed-reset approach, we will consider the process to end when the population of the main qubit reaches the minimum value of $p_g = 0.98$ for the first time, which is the instant when the interaction must be turned off. Still, the required time to reach the desired ground-state population, the reset time, is denoted t_{stop}.

Now, to study the reset protocol for the models presented in Figs. 1(c)–1(e), let us start considering the two-qubit model [Fig. 1(c)], where we analyzed the dynamics of the ground-state population of the main qubit for different values of the dissipation rate of the auxiliary qubit, given by γ. For this configuration, Fig. 2(a) shows the ground-state population versus gt. Looking at this panel, when considering the steady-state approach, we can notice that the best value is $\gamma = 10g$. Unlike what would be expected, as the dissipation rate is increased regarding to the coupling strength between the two qubits, the system reset becomes ineffective, i.e., the resetting will take longer to occur, e.g., see the curve for $\gamma = 20g$. Conversely, still in the same approach, if the dissipation rate is too small, it will take too long for the reset process to stabilize and finish, although the first peak of the dynamics occurs earlier, what is a good fact for the pulsed approach, as it happens for either $\gamma = 0.5g$ or $\gamma = 1g$ for instance.

Figure 2(b) shows the time gt_{stop} as a function of γ/g for the two reset approaches. Starting with the pulsed approach, we can see that for values of γ/g smaller than approximately 2, gt_{stop} does not depend on the decay rate of the auxiliary qubit, with the best times being close to $gt_{\text{stop}} = 1.45$. On the other hand, when considering the steady-state approach, from Fig. 2(a) we see that there is an optimum value for the reset time. From Fig. 2(b), we numerically find that this optimum value ($gt_{\text{stop}} \sim 2.08$) occurs for $\gamma/g \sim 2.13$. For values greater than this ratio, the reset process is ineffective since the time gt_{stop} increases as γ/g increases. Still, for $\gamma/g < 2$, the time also increases as the ratio γ/g decreases. For instance, if we now consider the minimum ground-state population of 0.995, which is required to perform realistic quantum computing, the best reset times achieved are $gt \sim 1.53$ and $gt \sim 2.60$ for the pulsed and steady-state approaches, respectively, where the parameter that optimizes the reset time for the latter approach is $\gamma/g \approx 2.59$.

Regarding the two-qubit model, we can see in Fig. 2(a) that the dynamics for greater values of γ do not oscillate, while the dynamics for smaller values of γ do oscillate, as we can see by comparing the curves for $\gamma = 20g$ and $\gamma = 0.5g$. These oscillations for the smaller values of γ, which arise from the energy flux between the qubits, are the origin of the discontinuities in Fig. 2(b) in the curve for the steady-state approach. In fact, at the beginning of the dynamics, the energy stored in the main qubit flows to the auxiliary qubit, which has a weak decay; that is, γ has the same magnitude as or is smaller than the coupling strength g. Then, due to its small dissipation rate, the energy that is transferred to the auxiliary qubit is able to flow back to the main one before it completely dissipates; hence, the ground-state population of the main qubit keeps recurring. This energy exchange between the qubits continues to occur, and several oscillations in the dynamics of the ground-state population take place until the reset process is over. It is worth noting that the number of oscillations depends on the value of γ; that is, the greater the number of oscillations is, the longer the reset time is and vice versa.

For the two-qubit–cavity model, represented in Fig. 1(d), we have three parameters, two from the Hamiltonian in Eq. (3) and one from the dissipation operator, which are, respectively, the coupling strength g between the two qubits, the coupling strength λ between the auxiliary qubit and the cavity mode field, and the damping rate κ of the electromagnetic field mode. Thus, by fixing the coupling g as before, two parameters remain to be adjusted in order to optimize the resetting process. The results for this case are shown in Fig. 3, where we plot in the top panels the dynamics of the ground-state population of the main qubit as a function of the dimensionless time gt for $\lambda = 1g$ [Fig. 3(a)] and $\lambda = 4g$ [Fig. 3(b)], in both cases considering different values for κ (see the legend). Looking at these two panels, once again, the previous discussion about steady-state approach applies since there are values of κ and λ for which the dynamics either oscillates and takes a long time to stabilize with a ground-state population above the predefined bound or does not fluctuate but still takes time to reach the desired bound. Hence, for this approach, once

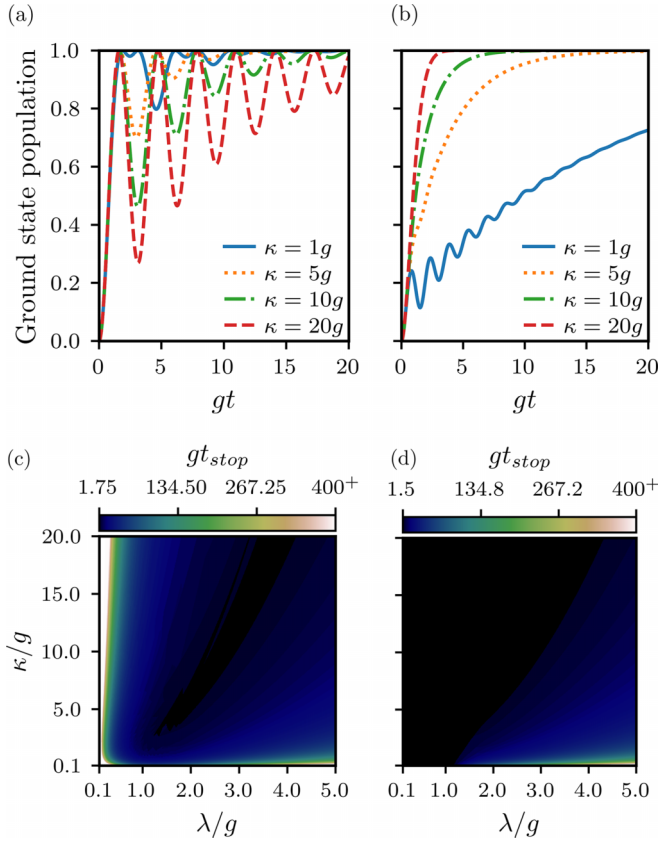

FIG. 3. Resetting process for the two-qubit–cavity model. In these simulations the initial state of the system is given by $\rho_M = |e\rangle\langle e|$, $\rho_A = |g\rangle\langle g|$, and $\rho_c = |0\rangle\langle 0|$, i.e., the main qubit, auxiliary qubit, and cavity mode, respectively. The top panels show the ground-state population of the main qubit as a function of the dimensionless time gt for two coupling strength values, (a) $\lambda = 1g$ and (b) $\lambda = 4g$, and different dissipation rates κ, as indicated in the legend. The bottom panels show gt_{stop} optimized according to the parameters λ/g and κ/g for the two reset approaches: (c) steady-state approach and (d) pulsed approach. In the blank areas in (c) and (d), the time needed to reset the system is higher than the limit time $gt_{\text{stop}} = 400$, although the reset still occurs for longer times.

more, we can infer that there is an optimum reset time. On the other hand, for the pulsed approach, an initial analysis reveals that the ratio between λ and κ appears to determine when the reset occurs since we can see from Fig. 3(a) (where we have the smaller value of λ, $\lambda = 1g$) that for all values of κ the dynamics reach their first peaks fast, whereas in Fig. 3(b) (where we have the bigger value of λ, $\lambda = 4g$) only the dynamics for the bigger values of κ reach their peaks fast.

Turning now to the optimizations, Fig. 3(c) shows gt_{stop} as a function of κ/g and λ/g for the steady-state approach. From this panel we can see that the best reset times (close to $gt_{\text{stop}} = 1.75$) are found in only a narrow range of the parameters λ and κ. We can also see that there are blank areas in this panel, which represent the set of parameters for which it is not possible to reach the minimum ground-state population of the main qubit ($p_g = 0.98$) in a stable way and within the maximum stipulated time in our simulations ($gt_{\text{max}} = 400$). For the pulsed approach, similar results can be seen in Fig. 3(d), but now the set of parameters with the best resetting times is larger, with the best times being around $gt_{\text{stop}} \approx 1.5$. On balance, for the first two configurations (the two-qubit model and two-qubit–cavity model), we found that the best times for the pulsed approach are slightly shorter than the best times for the steady-state approach. In contrast, the disadvantage of former compared to the latter approach is the need for a high level of precision in controlling the duration of the time pulse. In fact, since in the pulsed approach we have to stop the time evolution at a very precise time, we need an experimental precision of the order of $1/g$, meaning that even a small inaccuracy in the stopping time of the dynamics will cause the system state to be far from the ground state, thus introducing errors and making the resetting process ineffective. If we consider, like before, a minimum ground-state population of 0.995, the best reset times remain the same in both approaches. The changes in the results happen just in the set of parameters that reaches the required population; that is, the same best reset times are achieved, but a smaller set of parameters achieves the required population during these best times.

The IBM model [8] is the last configuration studied here. Again, since this model was developed aiming at the pulsed approach, we just searched for its optimization; that is, we did not consider the steady-state approach for this model. As said before, this model occurs in two steps. First, the population of the excited state $|e\rangle$ is transferred to the auxiliary state $|f\rangle$ via an auxiliary pulse. Since the intensity of the pulse modifies either the time spent in this step or the possible maximum transferred population, we consider here the same pulse that was used in [8], which takes approximately 75 ns to transfer the population to state $|f\rangle$. Once the main system is in state $|f\rangle$, the second step starts coupling the system to the dissipative cavity mode in order to bring it to the desired ground state. Hence, to optimize the second step of the approach and, consequently, the entire process, we searched for the parameters that make the dissipative dynamics of the transition $|g\rangle \leftrightarrow |f\rangle$ faster.

Proceeding as in the previous cases, in Figs. 4(a) and 4(b) we show the dynamics of the ground-state population of the main qubit as a function of the dimensionless time $\tilde{g}t$. Recalling that we are considering only the pulsed approach, from Fig. 4(a) we can see that, for a given value of $\Omega/\tilde{g}$, very large values of $\kappa/\tilde{g}$ do not improve the resetting process; that is, the higher $\kappa/\tilde{g}$ is, the longer the reset will take. However, by increasing $\Omega/\tilde{g}$, as shown Fig. 4(b), we see that the reset becomes faster because, as we can see by comparing Figs. 4(a) and 4(b), for a fixed $\kappa/\tilde{g}$, the first peak of the ground-state population happens earlier for $\Omega/\tilde{g} = 1.6\pi$.

Looking for the optimization process, Fig. 4(c) shows two regions. The colored region shows $\tilde{g}t_{\text{stop}}$ as a function of $\kappa/\tilde{g}$ and $\Omega/2\pi\tilde{g}$. Note from Fig. 4(c) that the shortest time spent in the second step of the reset is $\tilde{g}t_{\text{stop}} \approx 40.2$ (∼95.5 ns, when considering $\tilde{g}/2\pi = 67$ MHz as in [8]), which results in a total resetting time (i.e., considering the two steps of the approach) of 170.5 ns, thus decreasing the resetting time by almost 20% compared to the result achieved in Ref. [8], which is 210 ns. The other region is the blank area, which represents again the set of parameters whose resetting times are longer than the limit of $\tilde{g}t = 400$. For these parameters the resetting is delayed

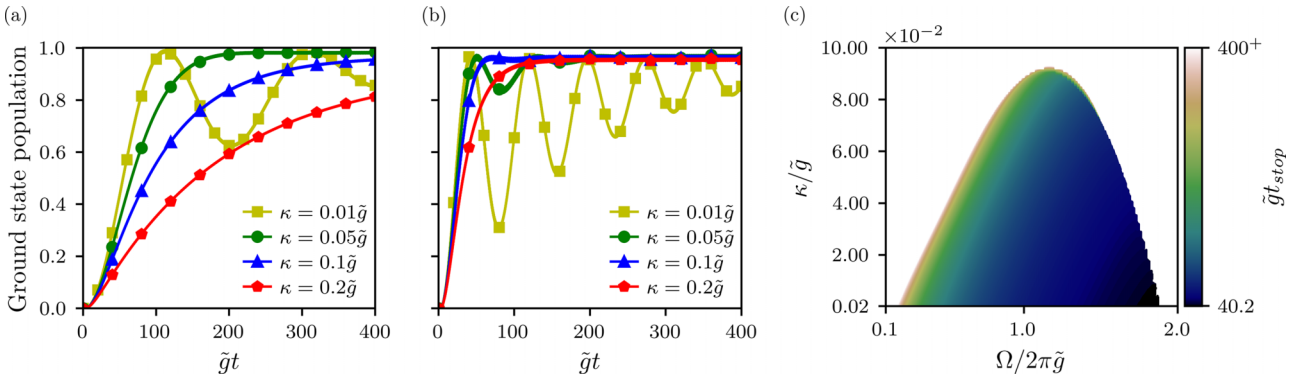

FIG. 4. Resetting process in the IBM model studied in [8]. In these simulations the initial state of the main system is $\rho_M = |f\rangle\langle f|$, while the initial state of the cavity mode is $\rho_c = |0\rangle\langle 0|$. We considered different dissipation rates $\kappa/\tilde{g}$, as indicated in the legend. (a) and (b) show the ground-state population of the main qubit as a function of the dimensionless time $\tilde{g}t$. The driven strengths in these plots are, respectively, $\Omega/\tilde{g} = 0.6\pi$ and $\Omega/\tilde{g} = 1.6\pi$. (c) shows $\tilde{g}t_{\text{stop}}$ as a function of the parameters $\Omega/2\pi\tilde{g}$ and $\kappa/\tilde{g}$. In the white area the time needed to reset the system is higher than the maximum stipulated time $\tilde{g}t_{\text{stop}} = 400$.

due to one of the following reasons: (i) The dynamics for a given $\Omega/2\pi\tilde{g}$ and $\kappa/\tilde{g}$ naturally take too long; this behavior occurs mostly for small values of Ω [e.g., see the curve for $\kappa = 0.2\tilde{g}$ in Fig. 4(a)]. (ii) As stated before, the efficiency of the transition $|g\rangle \leftrightarrow |f\rangle$ depends on the intensity of the pulse; therefore, as the value of $\Omega/2\pi\tilde{g}$ increases, the smaller the efficiency of this transition becomes, the longer the interaction between the qubit and the cavity has to continue until the bound population of $p_g = 0.98$ is reached, and occasionally, this time surpasses the predefined limit of $\tilde{g}t = 400$.

An important question that could rise is the impact on quantum computing of the lossy effects induced by the auxiliary systems in the dynamics because they can harm the performance of the device. When the main qubit is not working, some methods can be applied to reduce the cross talk due to the interaction of the main qubit and, consequently the reset components with the other working qubits. For example, following [30,31], the couplers present in the architecture of the computer can be used to reduce such cross talk and even effectively cancel the interactions between two specific components, which are the main qubit and other working qubits present in the architecture of the quantum device. On the other hand, when the main qubit is actively involved in calculation tasks, it is possible to set its frequency far off resonance, which implies a large detuning between the main and auxiliary qubits that cancels the interaction between them. Therefore, during either the resetting process or the computing step, it is possible to avoid the undesired cross talk and strong induced decay of the qubits.

For instance, consider coupling strengths close to the ones in Ref. [31], which are around $g/2\pi = 10$ MHz. The Purcell decay time for the two-qubit model [Fig. 1(c)] is expressed as $T_{\text{Purcell}} = (\Delta/g)^2\gamma^{-1}$, with Δ being the detuning between the main and auxiliary qubits during the computing step [32]. Thus, assuming that the effective decay induced by the auxiliary qubit is of the order of the natural decay of the main qubit, that is, of the order of 50 μs [8,33], we note that detunings of the order of 1.5 to 2.5 GHz will be required. For instance, for the steady-state approach, it is possible to achieve $T_{\text{Purcell}} = 50$ μs using detunings close to 2.5 GHz and sets of parameters ($\gamma/g \sim 0.5$) that result in reset times of approximately 20 ns. On the other hand, for the pulsed approach, it is possible to achieve $T_{\text{Purcell}} = 50$ μs considering detunings smaller than 1.5 GHz, even if the optimum set of parameters is used ($\gamma/g \sim 0.1$). It is noteworthy that the required detunings are feasible enough to guarantee these reasonable decay times [32,34,35]. Now, for the two-qubit–cavity model [Fig. 1(d)], it is necessary to take into account the effective decay rate of the component coupled to the main qubit. In the second model studied here, the auxiliary qubit has an effective decay rate due to its resonant coupling to the dissipative cavity mode, which is given by $\Gamma_{\text{eff}} = \lambda^2/\kappa$ [36,37], such that the Purcell decay time of the main qubit has to be computed as $T_{\text{Purcell}} = (\Delta/g)^2(\lambda^2/\kappa)^{-1}$. In this context, it is possible to achieve the same Purcell decay times as before, $T_{\text{Purcell}} = 50$ μs, considering, for the pulsed approach, detunings of approximately 1.5 GHz and the optimum set of parameters, while the steady-state approach requires detunings of approximately 2 GHz and sets of parameters that result in reset times smaller than 100 ns. Additionally, if we consider a coupling strength similar to the one used in the IBM paper [8], which is $\tilde{g}/2\pi = 67$ MHz, it is possible to achieve Purcell decay times around 1 μs when considering detunings smaller than 3 GHz, which are still feasible, and sets of parameters that result in reset times of approximately 100 ns.

IV. CONCLUSION

In this work we analyzed the optimization of the resetting time of superconducting qubits in three models: (i) the two-qubit model, in which the main qubit is coupled to a second dissipative one; (ii) the two-qubit–cavity model, composed of two interacting qubits with coupling strength g, with one being the main qubit and the other being the auxiliary qubit, which is coupled to a dissipative cavity mode; and (iii) the IBM model, in which a qubit and an auxiliary level are coupled to a dissipative bosonic mode. To study the resetting times in the first two models, we considered two different situations: the steady-state and pulsed approaches. The IBM model, which was designed to operate with only the pulsed approach, was

introduced in Ref. [8]. After the optimizations we were able to reduce the resetting time achieved in [8] by about 20% for this model, as they achieved 210 ns for the resetting time and here, using the same coupling strength $\tilde{g}/2\pi = 67$ MHz, we achieved a resetting time of 170.5 ns. Furthermore, we note that this best resetting time of the IBM model is two orders of magnitude larger than the best resetting times of the two other models analyzed here, which are less than 5 ns, when we consider the same coupling strength as before. In both models (i) and (ii), the pulsed approach is slightly faster than the steady-state approach. However, it is necessary to keep in mind a possible disadvantage of the first approach compared to the latter, as the pulsed approach requires high experimental accuracy in its execution to control the system dynamics. Finally, it is important to note that one could argue that it could be possible to achieve shorter reset times in practice just by employing even stronger couplings. However, the couplings between the subsystems cannot be increased arbitrarily once we might end up in the ultrastrong- and deep-strong-coupling regimes [38,39], which are the regimes in which the interaction energies between the subsystems are the same order as or even higher than the free energies of the subsystems. In these regimes the ground state of the system is an entangled state between the subsystems [40,41], with virtual photons that make it difficult to prepare the main qubit in its ground state alone.

ACKNOWLEDGMENTS

We acknowledge financial support from the following Brazilian agencies: Coordenação de Aperfeiçoamento de Pessoal de Nível Superior (CAPES), Financial Code 001; National Council for Scientific and Technological Development (CNPq), Grants No. 311612/2021-0 and No. 301500/2018-5; São Paulo Research Foundation (FAPESP), Grants No. 2019/11999-5, No. 2019/13143-0, No. 2022/10218-2, No. 2021/04672-0, and No. 2022/00209-6, and Goiás State Research Support Foundation (FAPEG). This work was performed as part of the Brazilian National Institute of Science and Technology for Quantum Information (INCT-IQ/CNPq) Grant No. 465469/2014-0.

[1] F. Kleißler, A. Lazariev, and S. Arroyo-Camejo, npj Quantum Inf. **4**, 49 (2018).
[2] W. Huang, C. H. Yang, K. W. Chan, T. Tanttu, B. Hensen, R. C. C. Leon, M. A. Fogarty, J. C. C. Hwang, F. E. Hudson, K. M. Itoh, A. Morello, A. Laucht, and A. S. Dzurak, Nature (London) **569**, 532 (2019).
[3] A. G. Fowler, M. Mariantoni, J. M. Martinis, and A. N. Cleland, Phys. Rev. A **86**, 032324 (2012).
[4] E. Dennis, A. Kitaev, A. Landahl, and J. Preskill, J. Math. Phys. **43**, 4452 (2002).
[5] D. E. Gottesman, Ph.D. thesis, California Institute of Technology (Caltech), 1997.
[6] C. Wang, J. Harrington, and J. Preskill, Ann. Phys. (NY) **303**, 31 (2003).
[7] T. Xin, S. Wei, J. Cui, J. Xiao, I. Arrazola, L. Lamata, X. Kong, D. Lu, E. Solano, and G. Long, Phys. Rev. A **101**, 032307 (2020).
[8] D. J. Egger, M. Werninghaus, M. Ganzhorn, G. Salis, A. Fuhrer, P. Müller, and S. Filipp, Phys. Rev. Appl. **10**, 044030 (2018).
[9] S. Barrett, K. Hammerer, S. Harrison, T. E. Northup, and T. J. Osborne, Phys. Rev. Lett. **110**, 090501 (2013).
[10] D. Ristè, J. G. van Leeuwen, H.-S. Ku, K. W. Lehnert, and L. DiCarlo, Phys. Rev. Lett. **109**, 050507 (2012).
[11] A. Blais, R.-S. Huang, A. Wallraff, S. M. Girvin, and R. J. Schoelkopf, Phys. Rev. A **69**, 062320 (2004).
[12] A. Wallraff, D. I. Schuster, A. Blais, L. Frunzio, R.-S. Huang, J. Majer, S. Kumar, S. M. Girvin, and R. J. Schoelkopf, Nature (London) **431**, 162 (2004).
[13] M. D. Reed, B. R. Johnson, A. A. Houck, L. DiCarlo, J. M. Chow, D. I. Schuster, L. Frunzio, and R. J. Schoelkopf, Appl. Phys. Lett. **96**, 203110 (2010).
[14] J. Tuorila, M. Partanen, T. Ala-Nissila, and M. Möttönen, npj Quantum Inf. **3**, 27 (2017).
[15] J. Tuorila, J. Stockburger, T. Ala-Nissila, J. Ankerhold, and M. Möttönen, Phys. Rev. Res. **1**, 013004 (2019).
[16] T. Chen, L. Wan, J. Qiu, H. Peng, J. Lu, and Y. Yan, J. Phys. B **54**, 135503 (2021).
[17] D. Basilewitsch, R. Schmidt, D. Sugny, S. Maniscalco, and C. P. Koch, New J. Phys. **19**, 113042 (2017).
[18] J. Fischer, D. Basilewitsch, C. P. Koch, and D. Sugny, Phys. Rev. A **99**, 033410 (2019).
[19] D. Basilewitsch, J. Fischer, D. M. Reich, D. Sugny, and C. P. Koch, Phys. Rev. Res. **3**, 013110 (2021).
[20] D. Basilewitsch, F. Cosco, N. L. Gullo, M. Möttönen, T. Ala-Nissilä, C. P. Koch, and S. Maniscalco, New J. Phys. **21**, 093054 (2019).
[21] P. Magnard, P. Kurpiers, B. Royer, T. Walter, J.-C. Besse, S. Gasparinetti, M. Pechal, J. Heinsoo, S. Storz, A. Blais, and A. Wallraff, Phys. Rev. Lett. **121**, 060502 (2018).
[22] IBM, the quantum experience, IBM Q Experience, https://research.ibm.com/quantum-computing.
[23] H.-P. Breuer and F. Petruccione, *The Theory of Open Quantum Systems* (Oxford University Press, Oxford, 2002).
[24] C. Hu (private communication).
[25] M. Pechal, L. Huthmacher, C. Eichler, S. Zeytinoğlu, A. A. Abdumalikov, S. Berger, A. Wallraff, and S. Filipp, Phys. Rev. X **4**, 041010 (2014).
[26] S. Zeytinoğlu, M. Pechal, S. Berger, A. A. Abdumalikov, A. Wallraff, and S. Filipp, Phys. Rev. A **91**, 043846 (2015).
[27] J. Chu *et al.*, Nat. Phys. **19**, 126 (2023).
[28] J. Johansson, P. Nation, and F. Nori, Comput. Phys. Commun. **183**, 1760 (2012).
[29] J. Johansson, P. Nation, and F. Nori, Comput. Phys. Commun. **184**, 1234 (2013).
[30] Y. Xu, J. Chu, J. Yuan, J. Qiu, Y. Zhou, L. Zhang, X. Tan, Y. Yu, S. Liu, J. Li, F. Yan, and D. Yu, Phys. Rev. Lett. **125**, 240503 (2020).

[31] C.-K. Hu, J. Yuan, B. A. Veloso, J. Qiu, Y. Zhou, L. Zhang, J. Chu, O. Nurbolat, L. Hu, J. Li, Y. Xu, Y. Zhong, S. Liu, F. Yan, D. Tan, R. Bachelard, A. C. Santos, C. J. Villas-Boas, and D. Yu, Phys. Rev. Appl. **20**, 034072 (2023).

[32] A. A. Houck, J. A. Schreier, B. R. Johnson, J. M. Chow, J. Koch, J. M. Gambetta, D. I. Schuster, L. Frunzio, M. H. Devoret, S. M. Girvin, and R. J. Schoelkopf, Phys. Rev. Lett. **101**, 080502 (2008).

[33] J. J. Burnett, A. Bengtsson, M. Scigliuzzo, D. Niepce, M. Kudra, P. Delsing, and J. Bylander, npj Quantum Inf. **5**, 54 (2019).

[34] M. D. Hutchings, J. B. Hertzberg, Y. Liu, N. T. Bronn, G. A. Keefe, M. Brink, J. M. Chow, and B. L. T. Plourde, Phys. Rev. Appl. **8**, 044003 (2017).

[35] N. T. Bronn, E. Magesan, N. A. Masluk, J. M. Chow, J. M. Gambetta, and M. Steffen, IEEE Trans. Appl. Supercond. **25**, 1 (2015).

[36] F. O. Prado, E. I. Duzzioni, M. H. Y. Moussa, N. G. de Almeida, and C. J. Villas-Bôas, Phys. Rev. Lett. **102**, 073008 (2009).

[37] R. J. de Assis, C. M. Diniz, N. G. de Almeida, and C. J. Villas-Bôas, Entropy **25**, 1430 (2023).

[38] F. Yoshihara, T. Fuse, S. Ashhab, K. Kakuyanagi, S. Saito, and K. Semba, Phys. Rev. A **95**, 053824 (2017).

[39] A. Mercurio, V. Macrì, C. Gustin, S. Hughes, S. Savasta, and F. Nori, Phys. Rev. Res. **4**, 023048 (2022).

[40] T. Shitara, M. Bamba, F. Yoshihara, T. Fuse, S. Ashhab, K. Semba, and K. Koshino, New J. Phys. **23**, 103009 (2021).

[41] F. Beaudoin, J. M. Gambetta, and A. Blais, Phys. Rev. A **84**, 043832 (2011).